BOUNDARY LAYER MEASUREMENTS AT SUPERSONIC NOZZLE THROATS

Thesis by

Merwin Sibulkin

In Partial Fulfillment of the Requirements

For the Degree of

Aeronautical Engineer

California Institute of Technology

Pasadena, California

1956

ACKNOWLEDGEMENTS

The author wishes to express his appreciation to Dr. H. W. Liepmann for his supervision and helpful suggestions.

The author is indebted to Carl Thiele for much of the design of the instrumentation and to A. Irving and D. Griffith for its construction.

The author is grateful to Mrs. Barbara Paul for typing the manuscript.

The financial support received from the Jet Propulsion Laboratory is gratefully acknowledged.

ABSTRACT

Wall static pressure measurements and boundary layer pitot pressure surveys were made near the throat of a flexible wall supersonic wind-tunnel nozzle at three settings having throat radii of curvature from 33 to 59 inches. It is found that the longitudinal static pressure gradient at the nozzle throat calculated from one-dimensional flow theory agreed with the measured wall static pressure gradient.

The boundary-layer velocity profiles at the nozzle throat are presented and discussed. The boundary layers were turbulent and 0.046 to 0.107 inch thick. It is found that the boundary-layer momentum thickness at the nozzle throat calculated using the momentum-integral-equation and several approximations agrees with the values determined from the measured boundary layer profiles. Finally, it is noted that in spite of the different static pressure gradients, the boundary-layer velocity profiles for the different nozzle settings are similar, and it is shown analytically that this similarity is to be expected.

TABLE OF CONTENTS

NOMENCLATURE

H	$\equiv \delta^*/\theta$
L^*	radius of curvature at nozzle throat $\equiv 2/(d^2t/dx^2)^*$
M	Mach number
M_s	nozzle exit Mach number
N	constant in equation $(u/u_1)=(y/\delta)^{1/N}$
p	static pressure
p_0	supply pressure
p_0'	pitot pressure
t	local height of nozzle
T	temperature
T_e	equilibrium temperature
T_0	(1) total temperature; (2) supply temperature
$\bar{T}$	defined by Equation (3)
u	velocity in x direction
u_*	shearing stress velocity $=\sqrt{\tau/\rho_w}$
x	distance parallel to wall
y	distance perpendicular to wall
β	free-stream velocity gradient at nozzle throat
γ	ratio of specific heats
δ	boundary layer thickness
δ_{log}	boundary layer parameter defined in text
δ^*	displacement thickness
θ	momentum thickness
ν	kinematic viscosity

ρ static density

τ wall shearing stress

Subscripts

1 local value at boundary layer edge

w local value at wall

Superscripts

* value at M = 1 (except δ^*)

- mean value (evaluated at $\bar{T}$)

I. ORIGIN OF EXPERIMENT

The use of the momentum-integral-equation method for calculating the boundary-layer thickness corrections for wind-tunnel nozzle contours is widely known and has been partially confirmed by experiment. More recently, the boundary-layer integral equations have been used to calculate the heat transfer to wind-tunnel and rocket nozzle walls having turbulent boundary layers (e.g. Ref. 1). In these cases the region of greatest interest is the nozzle throat where the heat transfer rates are greatest (since ρu is greatest there). The calculation of local heat transfer rates can be divided into two steps: (1) the calculation of the local boundary-layer momentum thickness (which gives the local shearing stress), and (2) the calculation of the ratio of heat transfer to shearing stress (e.g., by using some form of Reynolds analogy). While it is believed that the calculation of step 2 can be made with sufficient accuracy, no measurements were available to test the accuracy of the methods used in the calculation of step 1. Consequently, measurements were made at several supersonic-nozzle throats to study the boundary layers there and to test the values of throat momentum-thickness predicted by Reference 1.

II. EXPERIMENTAL TECHNIQUE

Measurements were made of the pitot tube pressure, p_0', across the boundary layer and of the static pressure, p, along the nozzle wall. Due to the undesirability of drilling holes in the highly stressed nozzle flexible plate, a boundary layer pitot probe was developed which could be supported from the tunnel test section. A schematic drawing and photographs of the probe are shown in Figure 1. The pitot tube is fixed to a cantilever beam which is free to move inside the body of the probe when the beam deflection cable is pulled. The deflection of the beam is sensed by a pair of strain gages glued to the beam, and is measured by a self-balancing bridge (using a modified Brown Electronik precision indicator). The bridge was set so that one instrument division equalled 0.0002 inch, as determined by calibrating the indicator reading against the movement of a micrometer screw; contact with the micrometer was determined by a sensitive electrical fouling circuit. The position of the wall was chosen as that probe deflection reading at which further movement of the beam towards the wall gave no corresponding decrease in the measured pressure; which showed that although the cable was bending the flexible beam, the tip of the pitot tube was at a fixed position in the flow (i.e., at the wall). The tip of the pitot tube was made of flattened hypodermic tubing and had an external height of 0.004 inch and a width of 0.025 inch. The minimum probe Reynolds number was 1600 (based on a length of 0.004 inch), which was large enough to avoid errors due to viscous effects.

The wall static pressure was measured by moving a 0.050 inch tube having four coplaner 0.008 inch holes along the nozzle wall (Fig. 2). The tube was moved by a simple screw and nut arrangement, and its position was read to 0.01 inch. Measurements were made (1) with the tunnel clear, and (2) with a dummy pitot probe installed over the tube to check the extent to which the probe disturbed the flow field.

III. DISCUSSION OF MEASUREMENTS

Measurements were made at three nozzle settings corresponding to test section Mach numbers, M_s, of 2.2, 3.3, and 3.8. The nozzle shape parameters and tunnel supply conditions are given in Table 1. Previous hot wire and pitot pressure measurements made about 30 inches upstream of the nozzle throat had shown that the boundary layer was turbulent at that point. The static pressure ratio, p/p_0, surveys are shown in Figure 3 where p_0 is the tunnel supply pressure and $x = 0$ is the nozzle geometric throat. It can be seen that the change in pressure due to the dummy pitot probe is small upstream of the probe body. The measured throat boundary layer pitot pressure ratio, p_0'/p_0, is plotted versus distance perpendicular to the wall, y, in Figure 4. Each profile represents three or more traverses of the boundary layer. The minimum distance, y, at which data were obtained for run 2 is greater than for runs 1 and 3 due to a misalignment of the pitot probe tip during run 2.

The velocity, u, in the boundary layer was calculated using the assumptions p = constant and T_0 = constant across the boundary layer. The value of p was taken from the static tube survey, and T_0 was taken as the wind tunnel supply temperature. The values of p/p_0' and u/u_1 versus y/δ are tabulated in Table II, and the values of u/u_1 versus y/δ, log u/u_1 versus log y/δ, and u/u_1 versus log y/δ are plotted in Figures 5, 6, and 7. The value of δ was chosen from Figure 4 as the distance y at which $p_0'/p_0 = 0.995$.

A straight line faired through the velocity data plotted on the log-log basis (Fig. 6) gives a slope of about 1/7.0 to 1/7.5. This

shows that the throat boundary layers were turbulent, and suggests that assuming a 1/7 power velocity profile in applying the momentum-integral-equation to the calculation of nozzle-throat boundary layer thickness should give good results.

Theoretical values of u/u_1 vs. y/δ were calculated from the incompressible turbulent velocity distribution of von Kármán

$$\frac{u}{u_1} = 5.75 \frac{u_*}{u_1} \log \frac{y}{\delta} + \frac{u_*}{u_1} \left(5.75 \log \frac{u_* \delta}{\nu_w} + 5.5 \right) \qquad (1)$$

evaluated for $u_* = \sqrt{\tau/\rho_w}$. The shearing stress τ was calculated from

$$\frac{\tau}{\bar{\rho} u_1^2} = 0.0126 \left(\frac{\bar{\nu}}{u_1 \theta} \right)^{1/4} \qquad (2)$$

which is the incompressible turbulent skin friction relation of Blasius modified by the evaluation of $\bar{\rho}$ and $\bar{\nu}$ at a mean temperature

$$\bar{T} \equiv \frac{T_1 + T_e}{2} \qquad (3)$$

The value of T_e was calculated using a recovery factor of 0.9. Combining equations (1) and (2) gives u as a function of y for the known values of the constants δ, θ, u_1, ρ_w, $\bar{\rho}$, and $\bar{\nu}$. The computed curves for runs 1 and 3 (Fig. 7) bracket the data and, although the measured flow was not incompressible, it is believed that this agreement implies that the wall shearing stress did not differ greatly from the values computed from Equation (2).

The tunnel operating conditions and the measured boundary layer parameters are summarized in Table I. A boundary layer thickness δ_{log} has been defined as the value of y at $u/u_1 = 1$ given by a straight line drawn through the data on a plot of log u/u_1 vs. log y. From Figure 6 it can be seen that for these measurements $\delta_{log}/\delta \cong 0.8$. Table I shows that the boundary layer parameters were nearly constant for the three runs. This would indicate (as do Figures 5 to 7) that the boundary layer profiles had a similar shape in spite of their having different static pressure gradients. This similarity will be discussed in section IV. From Table I it can be seen that the measured values of the boundary layer shape parameter, H, agreed with the theoretical values tabulated by Tucker (Ref. 2) for N = 7. A comparison of the measured and calculated values of θ/δ and δ^*/δ shows that the measured physical boundary layer thickness, δ , is greater than that given by theory. However, if the measured value of δ_{log} is used, the agreement is improved.

IV. COMPARISON WITH THEORY

A theoretical calculation of boundary layer growth along the wind tunnel nozzle was made by means of the boundary-layer momentum-integral-equation

$$\frac{d\theta}{dx} + \left(H + 2 - M_1^2\right) \frac{du_1}{dx} \frac{\theta}{u_1} = \frac{\tau}{\rho_1 u_1^2} \qquad (4)$$

using values of τ given by equation (2) and values of H and θ/δ from Reference 2 for N = 7. The calculation was started from a point about 30 inches upstream of the nozzle throat where previous measurements had shown the boundary layer to be turbulent and about 1/4 inch thick.

The boundary layer thickness at the nozzle throat was also estimated by the "throat approximation" formula (Ref. 1, Eq. 35 and Section IV-C)

$$\delta = 0.052 \frac{\left(\bar{z}^*\right)^{1/5} \left(t^* L^*\right)^{2/5}}{T_0^{1/10}}, \quad \theta = \frac{7}{72} \delta \qquad (5)$$

The calculated and measured values of θ and δ are plotted on Figure 8 against the measured values of the velocity gradient parameter β. The calculated values of β were obtained (assuming one-dimensional, isentropic flow; cf. Ref. 1, App. B) from

$$\beta \equiv \left(\frac{du_1}{dx}\right)^* = 41.0 \sqrt{\frac{T_0}{t^* L^*}} \qquad (6)$$

Equation (6) gave values of β which agreed within 2 percent (Table I) with the experimental values of β determined from the measured wall static pressure gradient (e.g., Fig. 3). It can be seen that the "throat approximation" for θ agrees with the more exact calculation, and that both calculations agree with the measured values. The measured values

of δ are higher than those calculated while the measured values of δ_{log} are in closer agreement with those calculated, as might be expected from the behavior of θ/δ as discussed in Section III.

It has been noted (Section III) that the non-dimensional boundary layer velocity profiles from the different nozzles are similar. It has been suggested (Ref. 3) that for incompressible flow the shape of the velocity profile depends on a parameter of the form $(\theta/\tau)(dp/dx)$ which is the ratio of pressure to the viscous forces acting on the boundary layer (cf. Eq. 4). Consideration of the "throat approximation" analysis of Reference 1, which is based on a linear velocity gradient $u_1 = \varphi x$, shows (Appendix A) that for a particular nozzle $(\theta/\tau)(dp/dx)$ does not vary with x; and, furthermore, that this constant value of $(\theta/\tau)(dp/dx)$ is independent of nozzle shape and supply conditions. The numerical value is

$$\frac{\theta}{\tau}\frac{dp}{dx} = -0.26 \qquad (7)$$

This result implies (1) that, neglecting the effects of compressibility and within the accuracy of the "throat approximation" analysis, the turbulent boundary layers near supersonic nozzle throats are equilibrium layers, in the sense of Reference 3; and (2) that the profiles should be similar since they have the same value of the equilibrium parameter. Since τ was not measured, it is not possible to check Equation (7) directly.

Although no other equilibrium boundary-layer profiles having favorable pressure gradients, $(\theta/\tau)(dp/dx) < 0$, are available with which to compare these throat profiles, a comparison can be made with the

turbulent pipe flow profile for which $(\theta/\tau)(dp/dx) \cong -0.19$ (Appendix B). It can be seen (Fig. 7) that for the throat profiles u is linear with log y almost to the outer edge of the boundary layer, which is also a well known characteristic of the pipe flow profile (Ref. 4). For flat plate flow, $(\theta/\tau)(dp/dx) = 0$, and for equilibrium flows with positive pressure gradients, the semi-logarithmic profile departs from linearity well within the boundary layer (Ref. 3, Fig. 18).

REFERENCES

1. Sibulkin, M., "Heat Transfer to an Incompressible Turbulent Boundary Layer and Estimation of Heat Transfer Coefficients at Supersonic Nozzle Throats", Jet Propulsion Laboratory Report No. 20-78, 1954.

2. Tucker, M., "Approximate Calculation of Turbulent Boundary-Layer Development in Compressible Flow", NACA TN 2337, 1951.

3. Clauser, F. H., "Turbulent Boundary Layers in Adverse Pressure Gradients", Journal of the Aeronautical Sciences, Vol. 21, No. 2, p. 91, 1954.

4. Goldstein, S., "Modern Developments in Fluid Dynamics", 1st Ed., Vol. 1, Fig. 93, Oxford University Press, London, 1938.

APPENDIX A: $(\theta/\tau)(dp/dx)$ FOR THROAT PROFILE

The basic analysis in Reference 1 assumes ρ = constant and

$$H = \frac{q}{T}, \quad \frac{\tau}{\rho u_1^2} = 0.0225 \left(\frac{\nu}{u_1 \delta}\right)^{1/4} \tag{A-1}$$

which combined with the momentum-integral-equation and the boundary condition $\delta(0) = 0$ gives

$$\delta^{5/4} = \frac{0.289\ \nu^{1/4}}{u_1^{11/28}} \int_0^x u_1^{27/7}\, dx_1, \quad \frac{\theta}{\delta} = \frac{7}{72} \tag{A-2}$$

In addition the "throat approximation" assumes

$$u_1 = \beta x \tag{A-3}$$

$$\delta = x = 0 \text{ at } u_1 = 0 \tag{A-4}$$

Assumptions (A-3) and (A-4) imply that

$$dp/dx = -\rho \beta^2 x \tag{A-5}$$

Combining Equations (A-1) through (A-4) gives

$$\theta = 0.0102\, \nu^{1/5} \beta^{-1/5} x^{3/5} \tag{A-6}$$

and

$$\tau = 0.0395\, \nu^{1/5} \rho^{4/5} \beta^{1/5} x^{1/5} \tag{A-7}$$

Combining Equations (A-5), (A-6), and (A-7) gives

$$\frac{\theta}{\tau} \frac{dp}{dx} = -0.26 \tag{A-8}$$

If one partially accounts for the variation of density in the real flow by taking $\rho = \bar{\rho}$ in Equation (A-1) and $\rho = \rho_1$ in Equation (A-5), the corresponding "quasi-incompressible" result is

$$\frac{\theta}{\tau} \frac{dp}{dx} = -0.26 \frac{\rho_1}{\rho} \tag{A-8a}$$

APPENDIX B: $(\theta/\tau)(dp/dx)$ FOR PIPE FLOW

For fully developed flow in a circular pipe

$$\frac{dp}{dx} = -\frac{2\tau}{r} \tag{B-1}$$

where r is the pipe radius. For turbulent, incompressible flow assuming a 1/7 power velocity profile

$$\frac{\theta}{r} = \frac{7}{72} \tag{B-2}$$

and therefore

$$\frac{\theta}{\tau}\frac{dp}{dx} = -0.19 \tag{B-3}$$

TABLE I. TUNNEL OPERATING CONDITIONS AND BOUNDARY-LAYER PARAMETERS

Run	M_s	t^* (in.)	L^* (in.)	p_0 (psia)	T_0 (°F)	M_1		
1	2.2	4.34	59	27.1	119	1.010		
2	3.3	1.45	34	27.1	102	0.984		
3	3.8	0.88	33	27.1	100	0.967		

Run	β (sec^{-1})		β (sec^{-1}) Eq. 6	δ (in.)	δ_{log} (in.)	θ (in.)	δ^* (in.)	$\frac{u_1\theta}{\bar{\nu}}$
1	742		730	0.107	0.082	0.0077	0.0130	4220
2	1615		1640	0.057	0.042	0.0037	0.0064	2010
3	2140		2160	0.046	0.036	0.0031	0.0054	1720

Run	H	H Ref. 2	θ/δ	θ/δ_{log}	θ/δ Ref. 2	δ^*/δ	δ^*/δ_{log}	δ^*/δ Ref. 2
1	1.69	1.74	0.072	0.094	0.091	0.122	0.158	0.158
2	1.74	1.72	0.064	0.088	0.091	0.112	0.153	0.157
3	1.72	1.70	0.068	0.087	0.091	0.118	0.150	0.156

TABLE II. BOUNDARY-LAYER PROFILE DATA

p/p_0'	u/u_1	y/δ	p/p_0'	u/u_1	y/δ	p/p_0'	u/u_1	y/δ
			Run 1					
			u_1 = 1086 ft/sec; δ = 0.107 in.					
0.523	1.002	1.077	0.521	1.003	1.548	0.736	0.704	0.066
0.521	1.002	2.200	0.521	1.003	2.112	0.699	0.758	0.104
0.521	1.002	1.824	0.580	0.924	0.416	0.707	0.747	0.094
0.521	1.002	1.454	0.596	0.901	0.350	0.714	0.737	0.086
0.522	1.000	1.077	0.603	0.891	0.321	0.544	0.972	0.654
0.537	0.980	0.705	0.620	0.869	0.267	0.534	0.985	0.751
0.607	0.887	0.310	0.632	0.853	0.234	0.528	0.993	0.844
0.669	0.800	0.150	0.651	0.827	0.188	0.524	0.998	0.941
0.563	0.946	0.517	0.681	0.784	0.128	0.522	1.000	1.028
0.527	0.992	0.892	0.730	0.714	0.066	0.522	1.000	1.123
0.522	1.000	1.272	0.722	0.724	0.076	0.742	0.695	0.061
0.522	1.000	1.653	0.693	0.766	0.113	0.742	0.695	0.057
0.522	1.000	1.276	0.678	0.788	0.139	0.747	0.687	0.053
0.522	1.000	1.366	0.666	0.806	0.162	0.754	0.676	0.049
0.522	1.000	1.548	0.656	0.819	0.180	0.761	0.667	0.046
0.522	1.000	1.175	0.649	0.829	0.197	0.769	0.654	0.042
0.531	0.989	0.789	0.687	0.776	0.122	0.776	0.643	0.037
0.579	0.924	0.421	0.722	0.724	0.076	0.783	0.632	0.034
0.721	0.726	0.078	0.730	0.713	0.068	0.788	0.624	0.030
0.632	0.852	0.236	0.746	0.689	0.057	0.793	0.615	0.026
0.549	0.966	0.611	0.759	0.669	0.048	0.794	0.614	0.024
0.523	0.999	0.981	0.776	0.642	0.037	0.794	0.614	0.022
0.521	1.003	1.366	0.795	0.612	0.022			

[a]Measurements are listed in chronological order.

TABLE II (cont'd). BOUNDARY-LAYER PROFILE DATA

p/p_0'	u/u_1	y/δ	p/p_0'	u/u_1	y/δ	p/p_0'	u/u_1	y/δ
				Run 2				
				u_1 = 1047 ft/sec; δ = 0.057 in.				
0.538	1.001	4.310	0.686	0.794	0.128	0.561	0.970	0.607
0.538	1.001	3.760	0.688	0.791	0.125	0.551	0.984	0.702
0.538	1.001	3.065	0.692	0.786	0.117	0.544	0.994	0.795
0.538	1.001	2.370	0.694	0.782	0.114	0.542	0.996	0.882
0.538	1.001	1.644	0.694	0.782	0.110	0.539	1.000	0.974
0.540	0.997	0.974	0.698	0.777	0.107	0.539	1.000	1.058
0.622	0.884	0.282	0.700	0.774	0.103	0.538	1.002	1.147
0.656	0.837	0.188	0.701	0.773	0.100	0.538	1.002	1.232
0.678	0.805	0.142	0.702	0.770	0.096	0.538	1.002	1.312
0.701	0.772	0.103	0.704	0.768	0.093	0.537	1.003	1.404
0.561	0.969	0.614	0.705	0.767	0.091	0.537	1.003	1.489
0.539	1.000	1.316	0.707	0.763	0.088	0.537	1.003	1.584
0.538	1.001	1.312	0.707	0.763	0.084	0.553	0.980	0.677
0.538	1.001	2.349	0.709	0.760	0.081	0.559	0.972	0.621
0.538	1.001	1.849	0.709	0.760	0.077	0.691	0.787	0.114
0.538	1.001	1.489	0.708	0.761	0.088	0.697	0.779	0.107
0.538	1.001	1.135	0.706	0.765	0.093	0.702	0.770	0.100
0.546	0.989	0.782	0.655	0.840	0.191	0.703	0.769	0.093
0.591	0.927	0.412	0.652	0.842	0.198	0.705	0.767	0.088
0.606	0.906	0.342	0.646	0.851	0.216	0.708	0.761	0.081
0.620	0.887	0.300	0.643	0.856	0.226	0.670	0.817	0.156
0.646	0.851	0.216	0.627	0.878	0.275	0.639	0.861	0.230
0.648	0.848	0.209	0.598	0.918	0.381	0.555	0.977	0.660
0.675	0.810	0.156	0.584	0.938	0.446	0.538	1.001	2.018
0.674	0.811	0.153	0.570	0.957	0.533			

[a]Measurements are listed in chronological order.

TABLE III (concluded). BOUNDARY-LAYER PROFILE DATA

p/p_0'	u/u_1	y/δ	p/p_0'	u/u_1	y/δ	p/p_0'	u/u_1	y/δ
			Run 3					
			u_1 = 1031 ft/sec; δ = 0.046 in.					
0.549	1.000	2.770	0.554	0.993	0.883	0.690	0.798	0.148
0.549	1.000	2.324	0.552	0.996	0.952	0.643	0.868	0.256
0.549	1.000	1.909	0.551	0.997	1.035	0.623	0.895	0.322
0.549	1.000	1.554	0.550	0.998	1.170	0.608	0.918	0.387
0.550	0.998	1.091	0.550	0.998	1.280	0.594	0.938	0.459
0.567	0.974	0.667	0.550	0.998	1.424	0.584	0.952	0.515
0.675	0.820	0.174	0.550	0.998	1.515	0.576	0.962	0.576
0.699	0.785	0.130	0.550	0.998	1.706	0.567	0.975	0.667
0.676	0.819	0.174	0.549	1.001	1.957	0.550	0.998	1.078
0.679	0.815	0.170	0.548	1.001	2.154	0.549	1.001	1.506
0.682	0.811	0.161	0.548	1.001	2.363	0.548	1.001	1.922
0.685	0.806	0.156	0.568	0.973	0.635	0.548	1.001	2.787
0.688	0.802	0.152	0.575	0.963	0.572	0.548	1.001	3.648
0.690	0.798	0.148	0.598	0.931	0.433	0.549	1.001	4.559
0.693	0.793	0.143	0.614	0.909	0.361	0.618	0.902	0.339
0.696	0.790	0.139	0.659	0.844	0.213	0.631	0.885	0.300
0.702	0.780	0.130	0.675	0.822	0.178	0.634	0.880	0.287
0.711	0.767	0.117	0.702	0.781	0.130	0.652	0.855	0.239
0.715	0.761	0.113	0.705	0.777	0.126	0.658	0.846	0.222
0.718	0.756	0.109	0.708	0.772	0.122	0.670	0.828	0.200
0.720	0.754	0.104	0.711	0.767	0.117	0.684	0.808	0.165
0.724	0.748	0.100	0.714	0.764	0.113	0.714	0.764	0.122
0.728	0.741	0.096	0.721	0.753	0.096	0.714	0.764	0.117
0.746	0.714	0.056	0.729	0.740	0.091	0.717	0.759	0.113
0.747	0.712	0.052	0.731	0.737	0.087	0.720	0.754	0.104
0.731	0.736	0.091	0.734	0.734	0.083	0.726	0.745	0.100
0.736	0.729	0.078	0.738	0.726	0.074	0.732	0.735	0.096
0.740	0.722	0.074	0.740	0.724	0.070	0.736	0.731	0.091
0.744	0.716	0.065	0.742	0.720	0.065	0.744	0.717	0.061
0.745	0.715	0.061	0.744	0.717	0.056	0.746	0.714	0.052
0.687	0.803	0.143	0.746	0.714	0.052	0.564	0.980	0.689
0.570	0.970	0.633	0.746	0.714	0.052	0.557	0.989	0.820
0.561	0.984	0.750						

[a]Measurements are listed in chronological order.

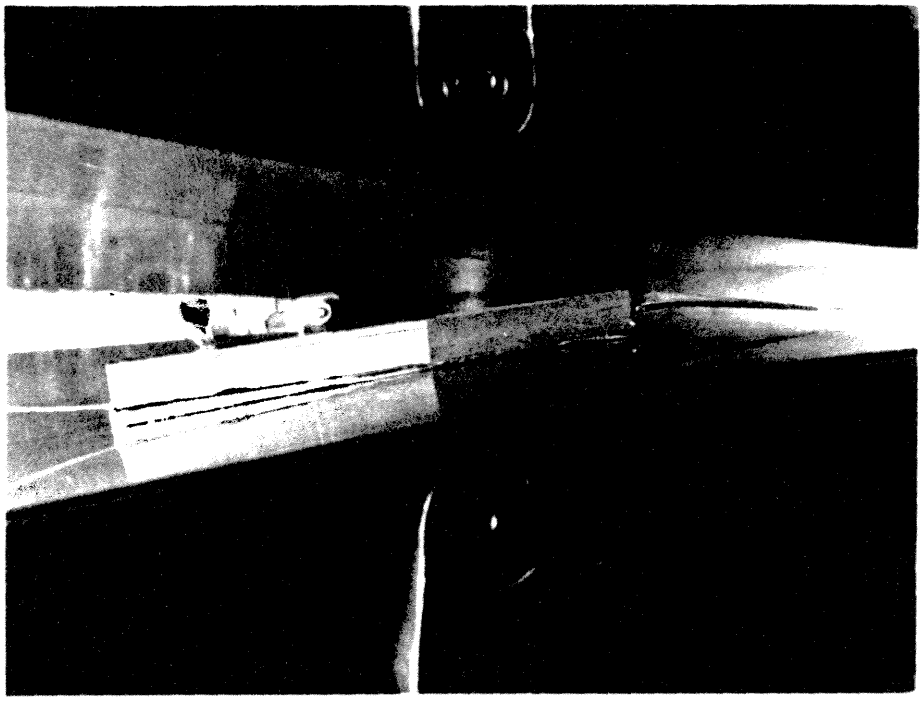

(a) PROBE IN WIND TUNNEL

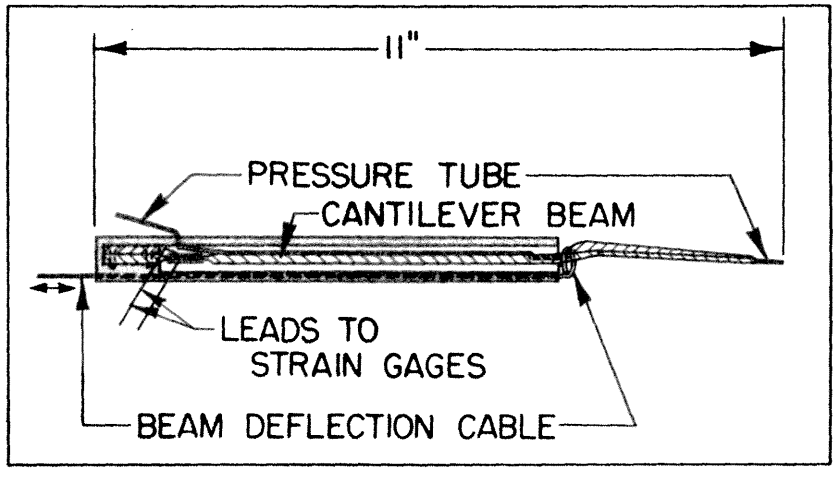

(b) SIDE VIEW (schematic)

Fig. 1. BOUNDARY-LAYER PITOT PROBE

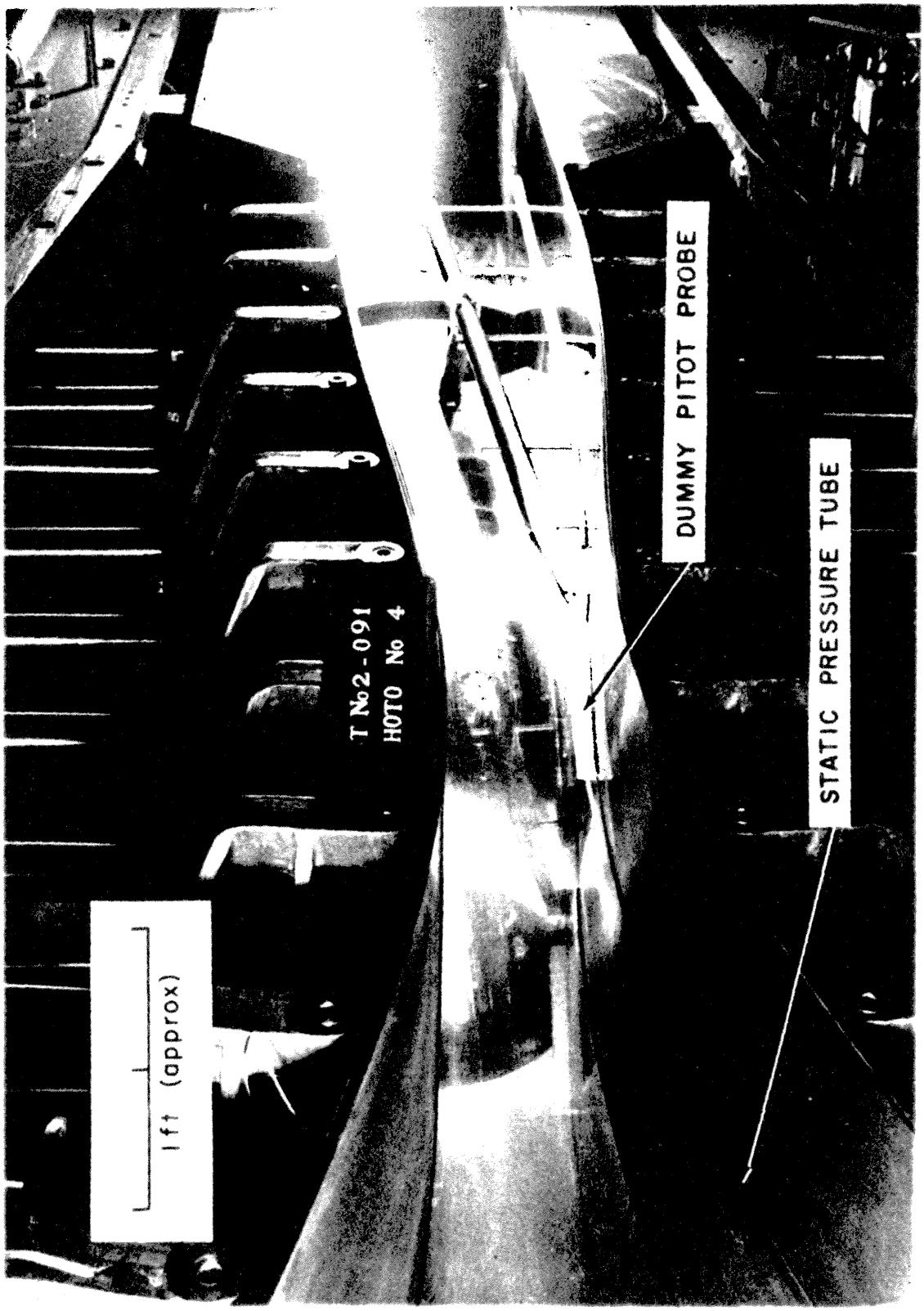

Fig. 2. STATIC-PRESSURE-TUBE INSTALLATION

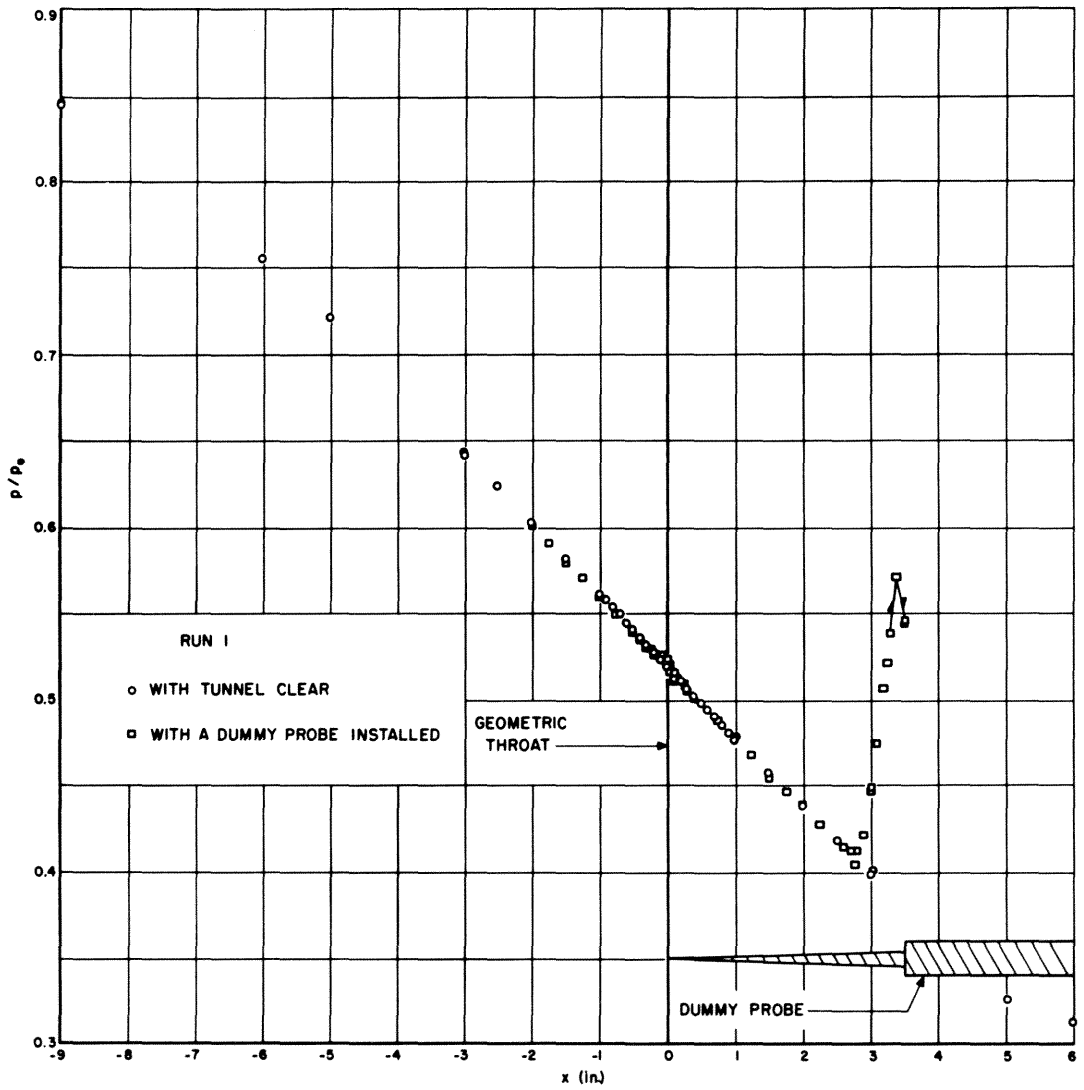

Fig. 3. WALL-STATIC-PRESSURE DISTRIBUTION

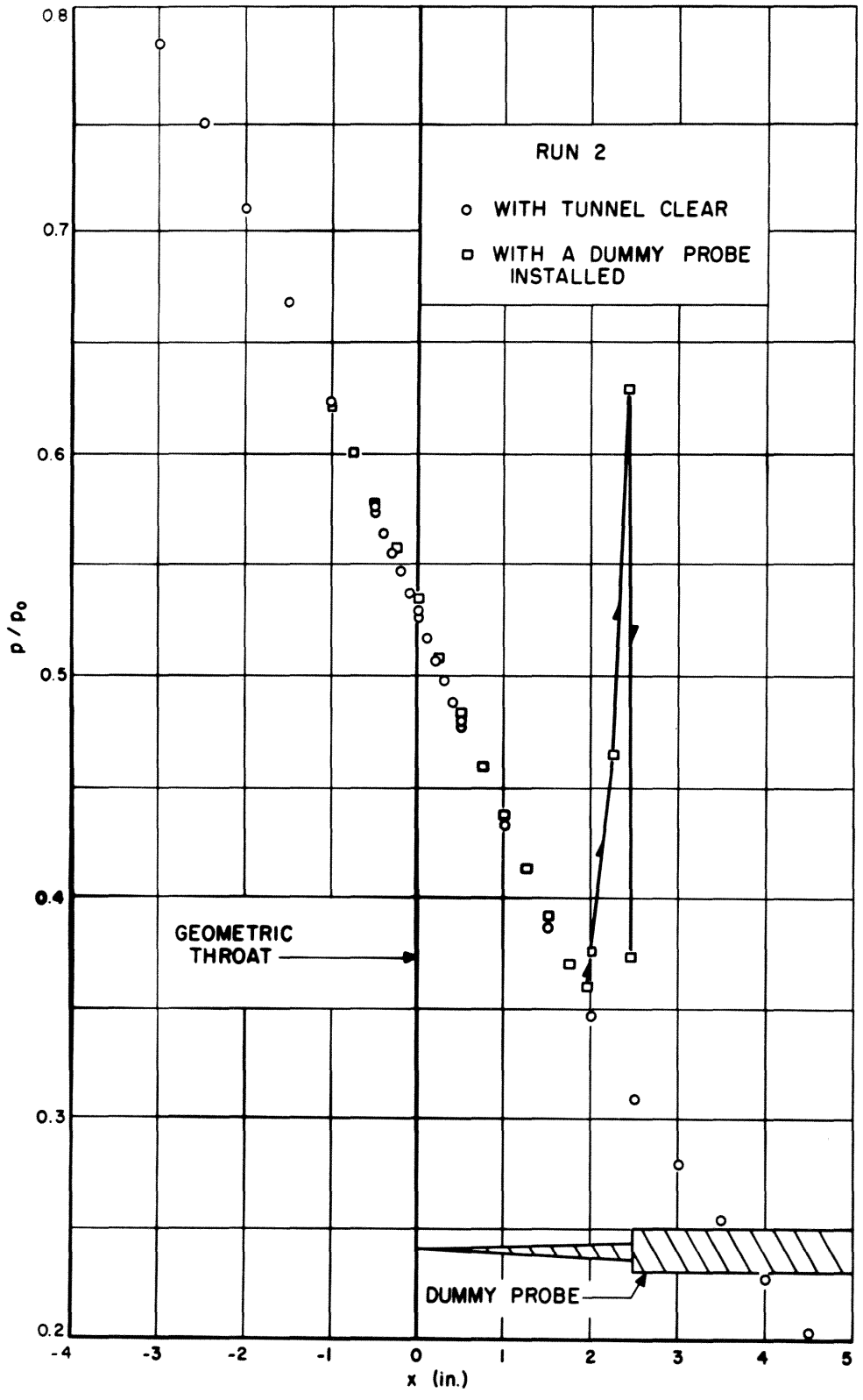

Fig. 3 (cont'd) WALL-STATIC-PRESSURE DISTRIBUTION

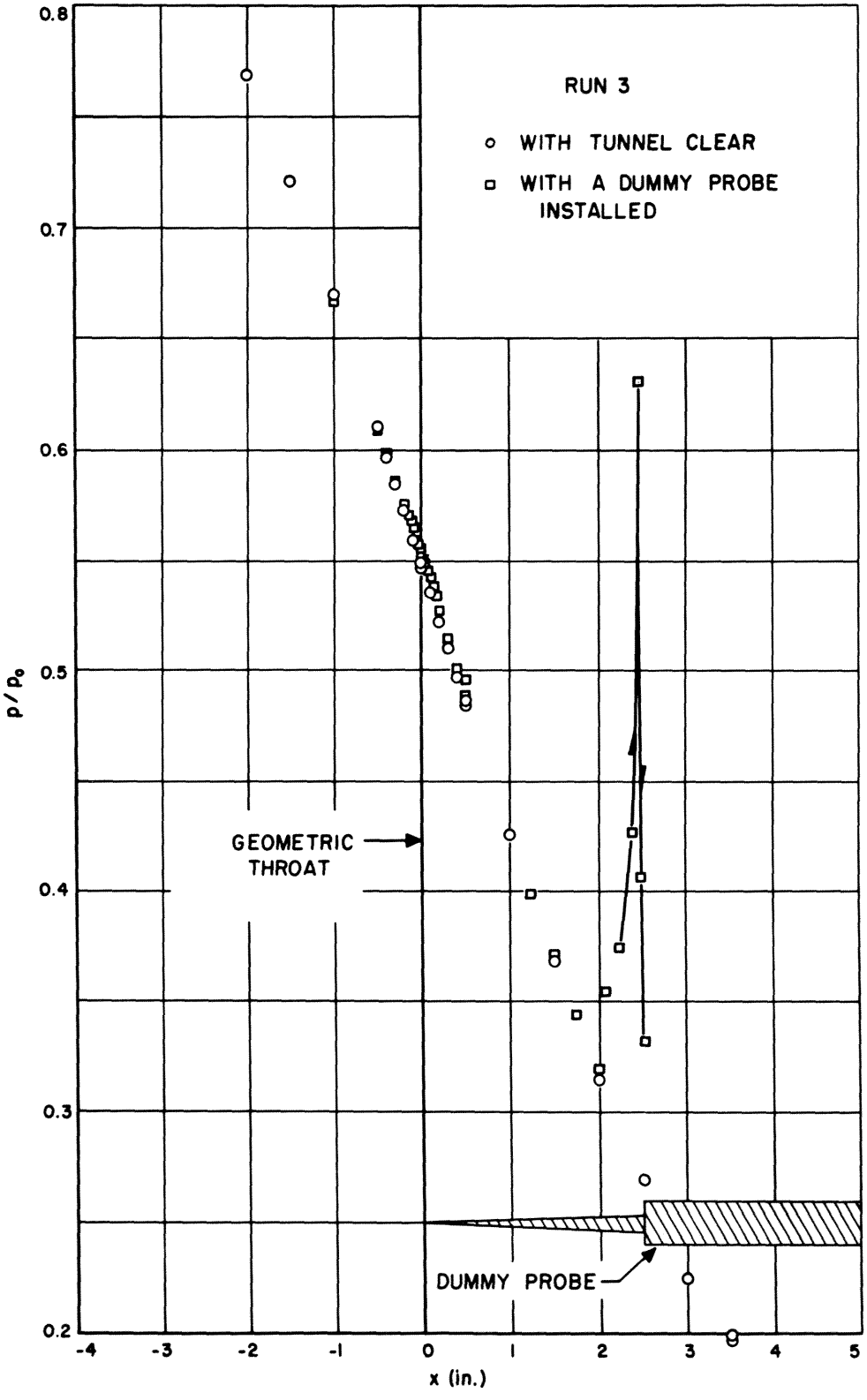

Fig. 3 (concluded) WALL-STATIC-PRESSURE DISTRIBUTION

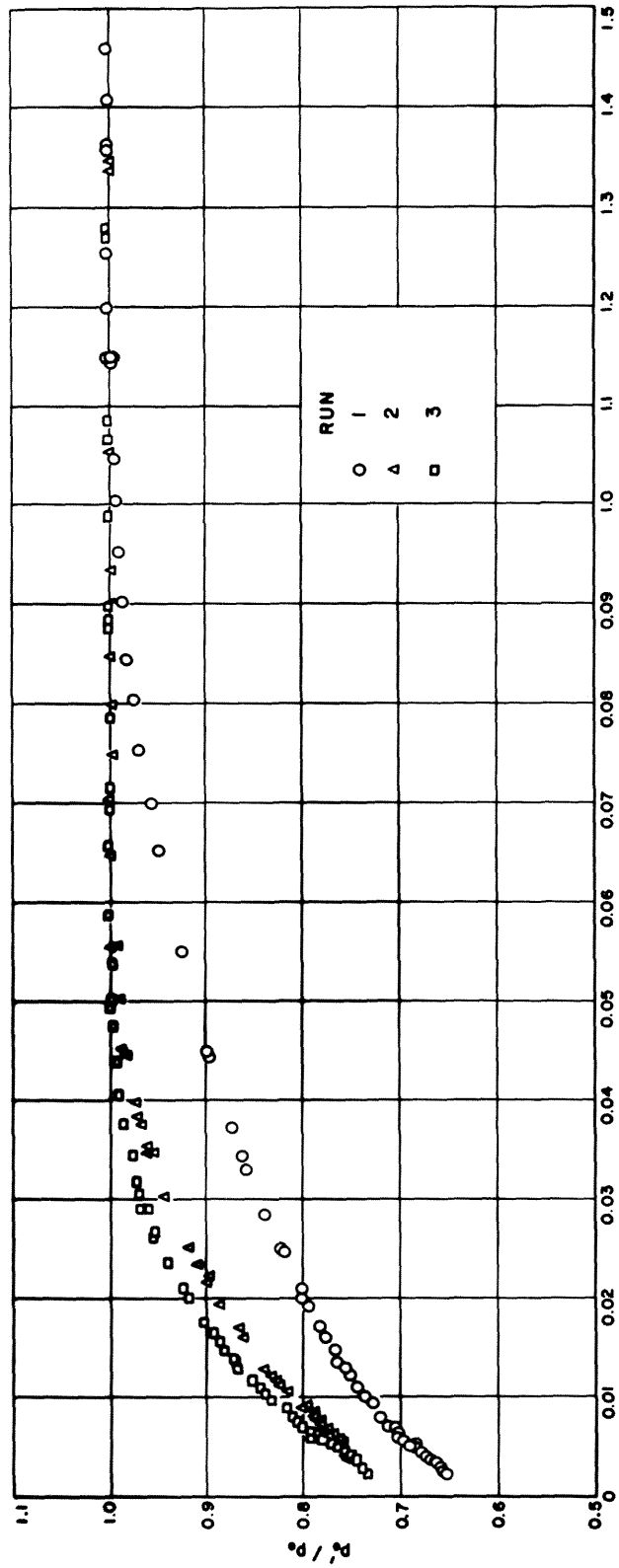

Fig. 4. BOUNDARY-LAYER-PITOT-PRESSURE DISTRIBUTION

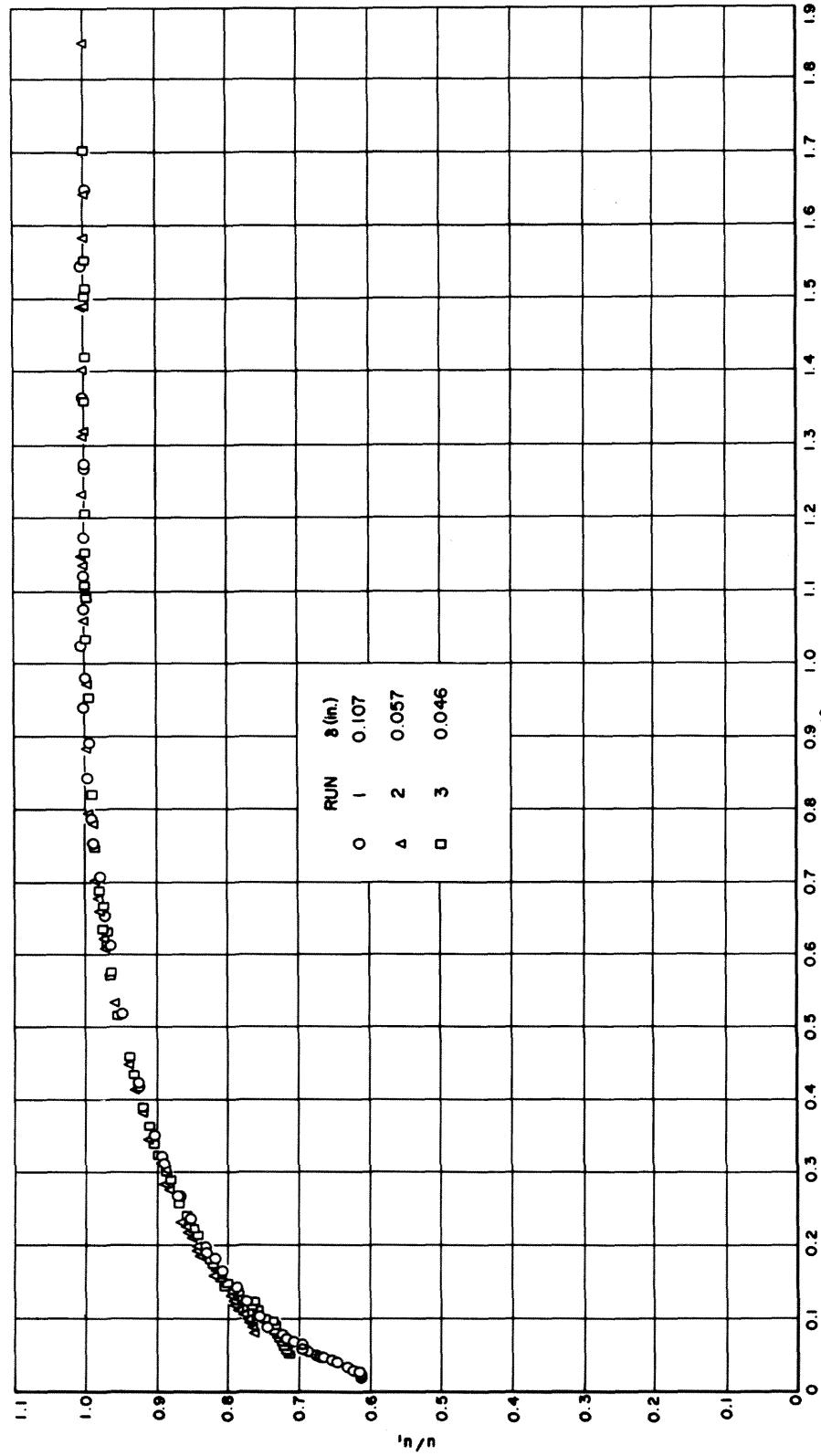

Fig. 5. BOUNDARY-LAYER-VELOCITY DISTRIBUTION

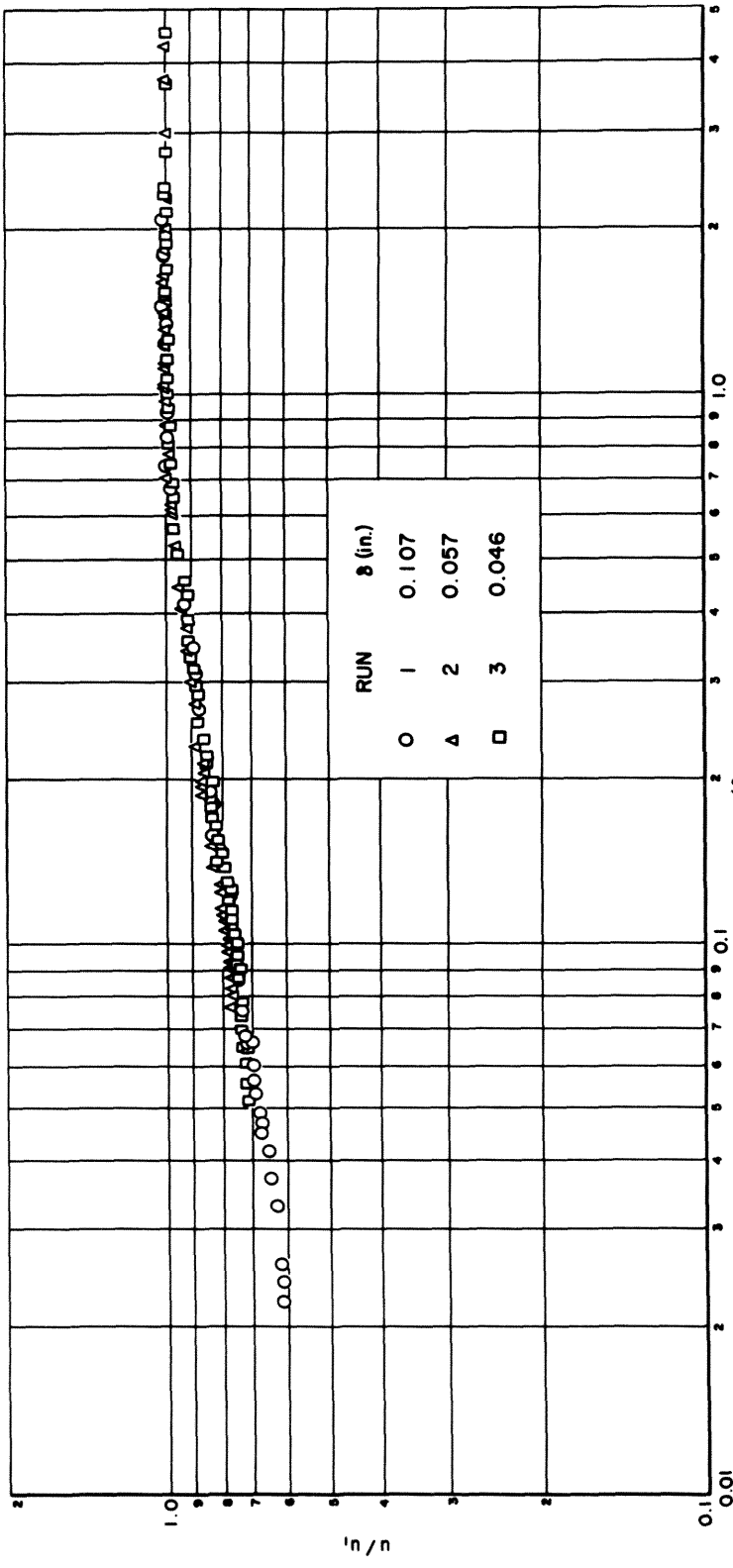

Fig. 6. BOUNDARY-LAYER-VELOCITY DISTRIBUTION PLOTTED WITH LOG-LOG COORDINATES

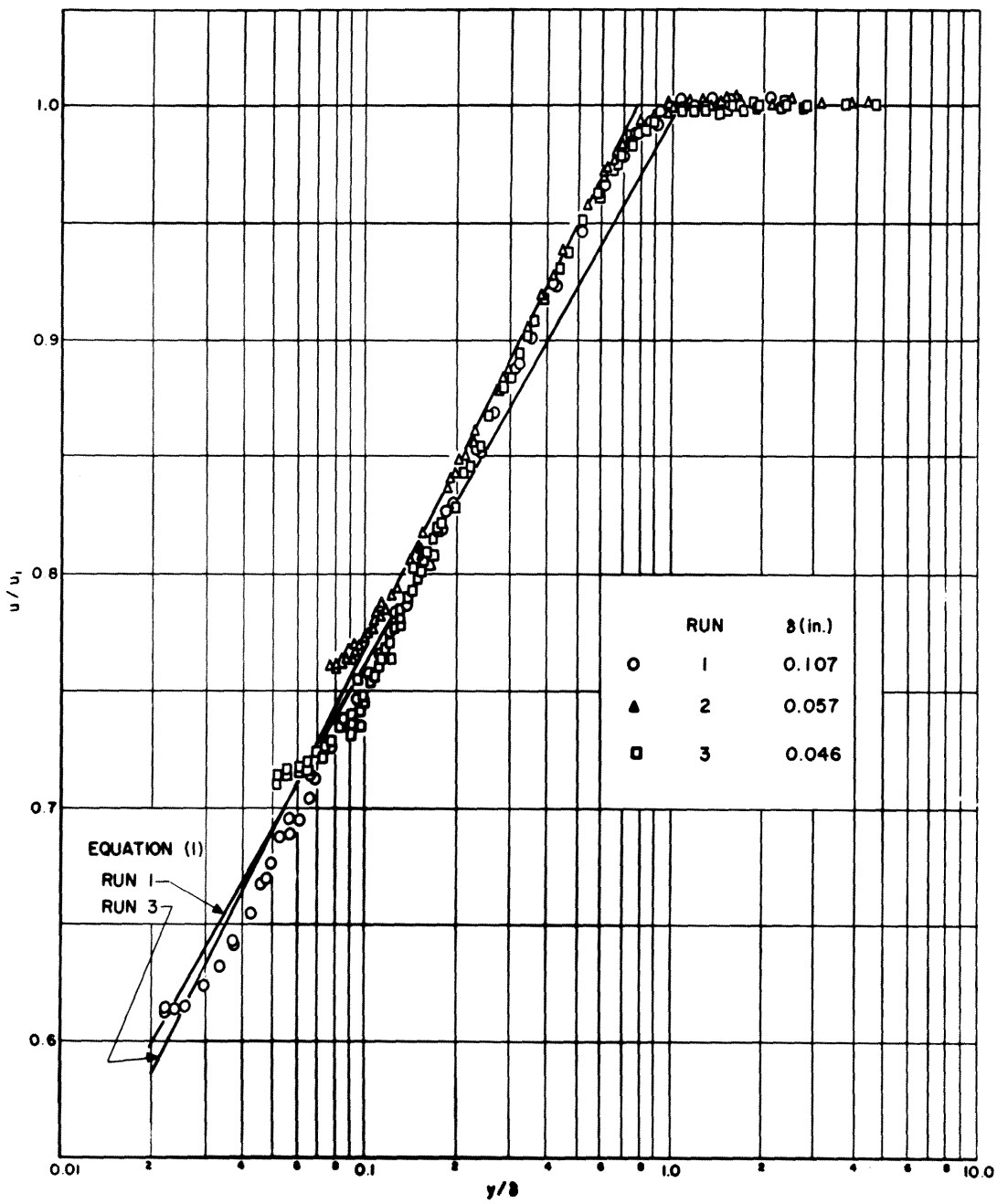

Fig. 7. BOUNDARY-LAYER-VELOCITY DISTRIBUTION PLOTTED WITH SEMI-LOG COORDINATES

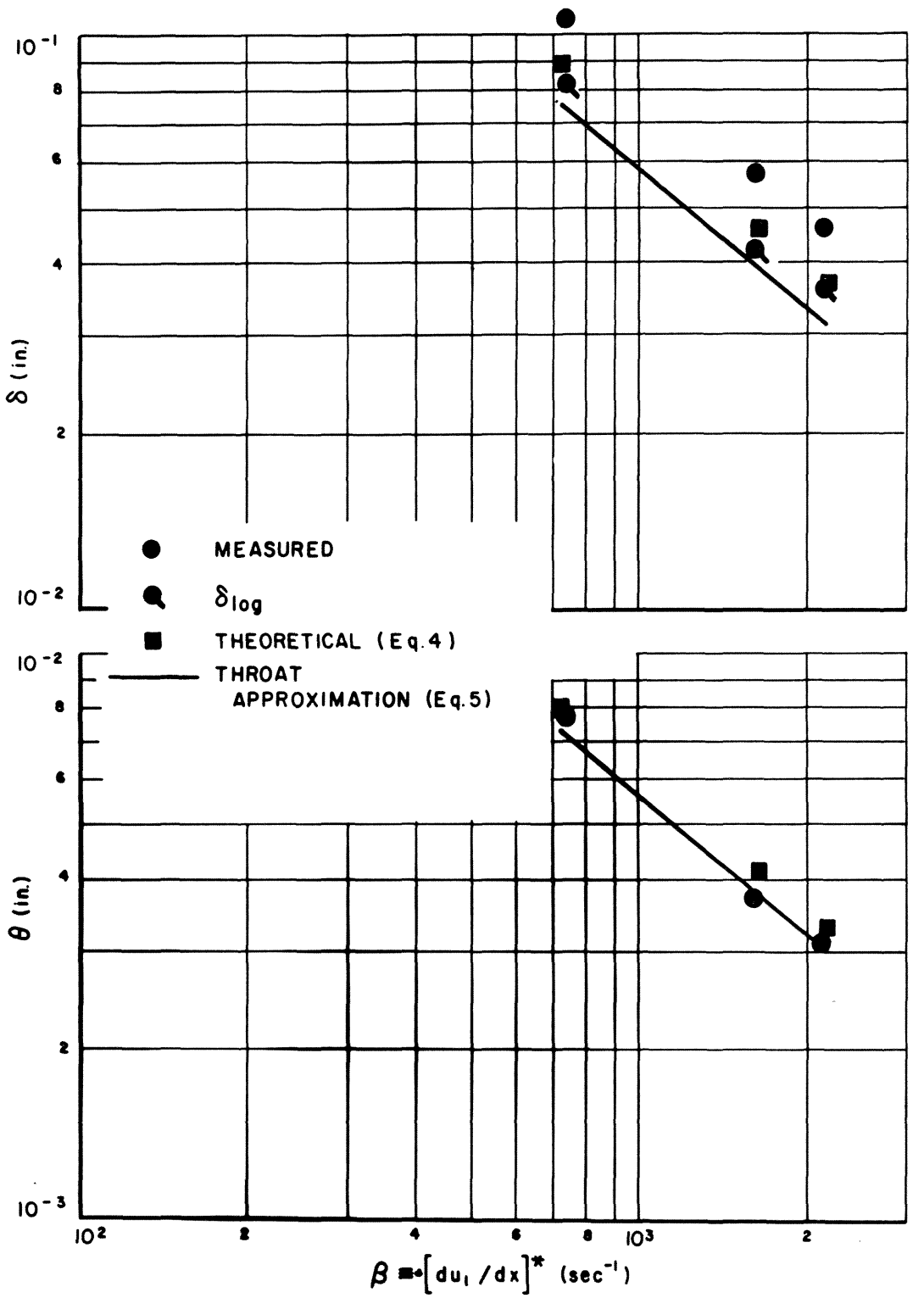

Fig. 8. COMPARISON OF MEASURED AND CALCULATED BOUNDARY-LAYER THICKNESSES